Infrared Physics & Technology 140 (2024) 105389

Contents lists available at ScienceDirect

Infrared Physics and Technology

journal homepage: www.elsevier.com/locate/infrared

Research Paper

Optical absorption spectra in the far-infrared range and phonons of $CdSe_{1-x}Te_x$ thin films

Andrii I. Kashuba [a], Leszek Bychto [b], Krzysztof Dorywalski [c], Roman Petrus [d], Alexander Veber [e,f], Ljiljana Puskar [e], Ulrich Schade [e], Ihor V. Semkiv [a], Bohdan Andriyevsky [b,*]

[a] Department of General Physics, Lviv Polytechnic National University, Bandera Str. 12, 79013 Lviv, Ukraine
[b] Faculty of Electronics and Computer Sciences, Koszalin University of Technology, Śniadeckich Str. 2, PL-75-453, Koszalin, Poland
[c] Institute of Experimental Physics, Faculty of Mathematics, Physics and Informatics, University of Gdańsk, Wita Stwosza 57, 80-308 Gdańsk, Poland
[d] Carl Von Ossietzky University of Oldenburg, Institute of Physics, Carl-von-Ossietzky-Straße 11, 26129 Oldenburg, Germany
[e] Institute for Electronic Structure Dynamics, Helmholtz-Zentrum Berlin für Materialien und Energie GmbH, Albert-Einstein-Strasse 15, 12489 Berlin, Germany
[f] Department of Chemistry, Humboldt Universität zu Berlin, Brook-Taylor-Straße 2, 12489 Berlin, Germany

ARTICLE INFO

Keywords:
Semiconductors
$CdSe_{1-x}Te_x$ thin films
$CdSe_{1-x}Te_x$ crystals
Phonon spectra
DFT-based calculations
Dielectric function

ABSTRACT

Optical reflection spectra of $CdSe_{1-x}Te_x$ thin films deposited on quartz substrates are measured using the synchrotron radiation in the spectral range of 20–500 cm^{-1}. The absorption bands of CdSe, CdTe, $CdSe_{0.75}Te_{0.25}$, $CdSe_{0.5}Te_{0.5}$, and $CdSe_{0.25}Te_{0.75}$ films are localized in the range of 20–220 cm^{-1}. The imaginary parts of the dielectric function $\varepsilon_2(\lambda^{-1})$ of $CdTe_{1-x}Se_x$ crystals calculated in the framework of the density functional theory are in good agreement with the experimental reflection spectra of $CdTe_{1-x}Se_x$ films. The eigenvectors of the dynamical matrix $CdTe_{1-x}Se_x$ crystals are analyzed for several phonon modes to understand the difference between the frequency dependences of the calculated vibration density of states and the imaginary part of dielectric function $\varepsilon_2(\lambda^{-1})$. Small features of the experimental reflective spectra of $CdSe_{1-x}Te_x$ films in the ranges 50–70 cm^{-1} and 80–120 cm^{-1} are explained using the analysis of results of the molecular dynamics. During comparative molecular dynamics calculations, it was found that the vibration density of states of a thin CdTe slab with a surface-to-volume number of atoms relation of $N_S/N_V = 0.2$, experienced a redshift of approximately 30 cm^{-1}. This shift was observed in comparison with the CdTe single crystal.

1. Introduction

CdTe-based solar cells are one of the leading technologies of solar energy production due to their significant photovoltaic (PV) conversion efficiency, performance stability, low costs of fabrication, and short payback time [1]. In recent years PV modules and research-based small area devices based on CdTe solar cells have seen a significant increase in the efficiencies up to 18.6 % and 22.1 % [2]. The high solar cell efficiency (22.1 %) was achieved by using $CdSe_{1-x}Te_x$ solid state solutions (SSS), which have a lower band gap than CdTe [3]. Therefore CdSeTe SSS is one of the promising materials to improve the photovoltaic characteristics of thin-film solar cells [4 –6]. This improvement is possible because the band gap of CdTe thin films is ~ 1.5 eV and CdSe thin films is ~ 1.7 eV, while the band gap of $CdSe_{1-x}Te_x$ SSS is in the energy region 1.3–1.7 eV, which provides better efficiency compared to single CdTe absorber layer [7 –10]. Moreover, the band gap dependence of $CdSe_{1-x}Te_x$ is characterized by the bowing effect [9], which causes a smaller band gap compared to binary CdSe and CdTe. Therefore the CdSeTe/CdTe bilayer absorbs photons with longer wavelengths, which improves the photovoltaic characteristics. In addition, selenium contained in the CdSeTe/CdTe bilayer passivates bulk defects in the absorber, leading to increased device performance [11].

$CdSe_{1-x}Te_x$ SSS crystallizes in both the zinc blende and the wurzite structures [9,12,13]. However, for solar cell application only the zinc blende structure of $CdSe_{1-x}Te_x$ is desired because it is photoactive and can convert light into photocurrent, whereas the wurzite structure is not photoactive [12]. For $CdSe_{1-x}Te_x$ thin films the characteristics of band gaps [9,14], phase transition [15,16], photoconductivity [17],

* Corresponding author.
E-mail addresses: andrii.i.kashuba@lpnu.ua (A.I. Kashuba), leszek.bychto@tu.koszalin.pl (L. Bychto), krzysztof.dorywalski@ug.edu.pl (K. Dorywalski), roman.petrus@uol.de (R. Petrus), alexander.veber@helmholtz-berlin.de (A. Veber), ljiljana.puskar@helmholtz-berlin.de (L. Puskar), ulrich.schade@helmholtz-berlin.de (U. Schade), semkiv.igor.5@gmail.com (I.V. Semkiv), bohdan.andriyevskyy@tu.koszalin.pl (B. Andriyevsky).

https://doi.org/10.1016/j.infrared.2024.105389
Received 14 February 2024; Received in revised form 31 May 2024; Accepted 4 June 2024
Available online 5 June 2024

photoactivity [12], and electrical properties [18,19] of $CdSe_{1-x}Te_x$ films have been studied.

Among the numerous studies on the optical properties of $CdSe_{1-x}Te_x$ SSS, the reference information on the optical properties in the far-infrared range is somewhat limited [20 –22]. One of the interesting studies on this problem is Ref. [23], where the experimental Raman and infrared spectra are compared with the vibration spectra of CdSe/CdS core/shell nanoplatelets calculated from first principles using the density functional theory (DFT). On the other hand, the optical properties of $CdSe_{1-x}Te_x$ SSS in the far-infrared range have not been sufficiently studied.

Because of the small dimensions used in modern semiconducting devices, thin film technology is the prevailing one. The significant parameters of the deposited thin films are the polycrystalline grain dimensions and the electrical conductivity caused by the shallow electronic states originating from structural defects. It is known that the well-crystallized polycrystalline sample with several micrometer grain size can be treated as a bulk/infinite crystal for most practical purposes. If however, the grain dimensions are less than typically 20 lattice parameters the quantum confinement effects may be noticeable also in the vibrational spectra [24].

For CdSe quantum dots, the observed Stokes shift of the LO-phonon Raman peak was found to be 206.1 cm^{-1}, which is smaller than the corresponding bulk sample value of 210 cm^{-1} ([Ref. [25]]) by 3.9 cm^{-1}. According to Ref. [26], the latter shift originates from two sources: a redshift due to confinement of the optical phonons [27], which is expected to be 4.7 cm^{-1} for 4-nm large CdSe particles, and a blue shift caused by lattice contraction [28]. The lattice contraction takes place for the surface part of the polycrystalline grains, which leads to the blue shift in phonon spectra. Both effects occur for the relatively small grain dimensions. Competition of these two effects results in the final value of the vibration frequency of the thin film material observed in the experiment.

Information on the electrical conductivity of thin semiconducting films can be obtained by the analysis of their IR spectra. Depending on the magnitude of the free electron concentration N_c in the samples, the spectral features corresponding to the plasma reflection are expected to appear at different parts of the spectrum. The corresponding electron plasma frequency ω_p and the characteristic monotonous frequency decrease of the reflective coefficient ($dR/d\omega < 0$) may be detected in the spectral range $\omega > 30$ cm^{-1} for the free electron concentration $N_c > 10^{16}$ cm^{-3} [29].

In this work, experimental and theoretical studies of the optical properties of $CdSe_{1-x}Te_x$ films are carried out in the far-infrared range corresponding to the phonon excitations in the films.

2. Methods of experimental and DFT-based studies of materials

Measurements of the specular reflectance of $CdSe_{1-x}Te_x$ films deposited on the quartz layers were performed at an angle of incidence angle of 9° using the synchrotron radiation of BESSY II storage ring at the IRIS beamline of HZB (Berlin). The corresponding optical scheme of the measuring setup is presented in Fig. 1.

The thicknesses of the deposited CdSeTe layers were in the range of 0.44–1.2 μm. The high brilliance of the synchrotron radiation together with a Fourier-transform infrared (FTIR) Bruker Vertex 70/v spectrometer allows for a precise measurement of reflection spectra of the samples by applying a quasi-normal incidence set-up as further described in [30] with a gold film as reference. Measurements could be performed with undefined polarization of the radiation due to the isotropy of the samples. Samples were placed in a cryostat for measurement at ambient temperature and 5 K, near the liquid helium temperature. Spectra were recorded with a mechanically cooled transition edge superconducting bolometer (QMC) in the spectral range between 20 and 500 cm^{-1} with a resolution of 4 cm^{-1}. The FIR detector used was a Cryogen-free THz bolometer made by QMC instruments. It is a closed cycle Niobium transition-edge sensor (TES) superconducting bolometer.

The here-discussed reflection spectra are the result of the reflections from the air-film and the reflections from the film-substrate interface. Due to the low film thickness, the reflection spectra may not represent the expected complex reflection feature from the bulk material of the film but rather may indicate the absorption site within the film. Exemplarily, coherent model calculations (see Fig. 2) for a 1-μm thick film on quartz using published optical constants for CdTe [31] and the refractive index $\tilde{n} = 2 + i0$ for fused quartz results in a reflection feature with a reflective maximum at the wave number $\lambda^{-1} = 138.9$ cm^{-1}, which is a bit smaller than the corresponding value 141–143 cm^{-1} for the maximum of the strongest lattice absorption for the bulk CdTe [31].

The DFT calculations of the crystals studied were performed using the VASP code [33 –38] with the projector augmented wave pseudopotentials [38]. Two kinds of Perdew-Burke-Ernzerhof exchange-and-correlation functionals, GGA-PE and GGA-PS [39], were used. The dielectric functions in the range of phonon excitations $\varepsilon(\lambda^{-1})$ (here λ^{-1} is a wavenumber) were calculated in the framework of the density-functional-perturbation theory (DFPT), where the dynamical matrix is constructed and diagonalized and the phonon modes and frequencies/wavenumbers of the crystal are reported in the VASP output file. The cut-off energy for the plane waves of 500 eV, a

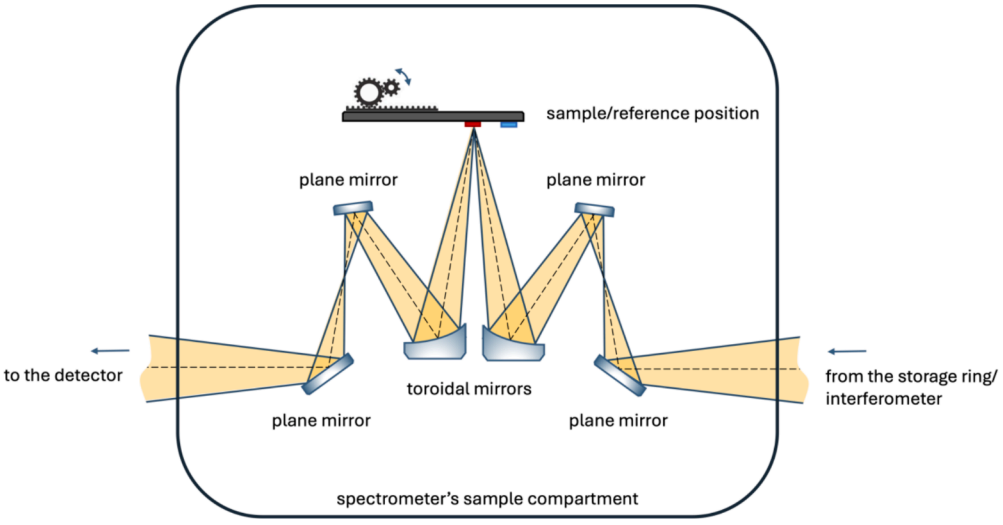

Fig. 1. Optical scheme of setup for the reflection spectra measurement of samples using FTIR spectrometer at IRIS beamline of BESSY II storage ring.

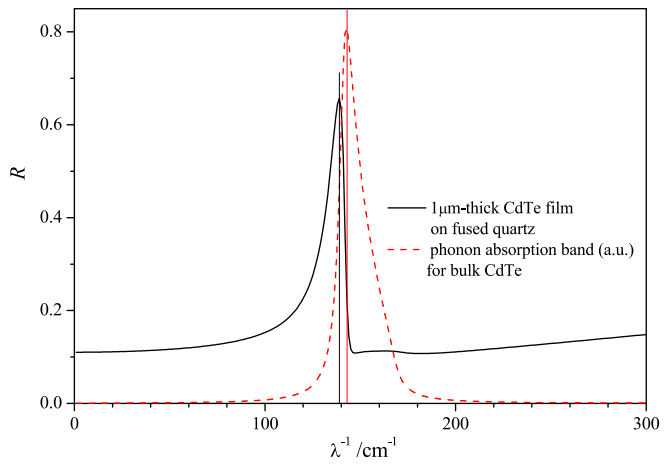

Fig. 2. The absorption band of bulk CdTe (red lines) [31] in comparison to the appearing reflectance of a 1-μm-thick CdTe film (black lines) as calculated from an optical layer model [32]. (For interpretation of the references to colour in this figure legend, the reader is referred to the web version of this article.)

Methfessel–Paxton smearing of 0.05 eV [40], and 10 irreducible K-points, because of the large supercell, were used for the calculations. The relaxations of the electronic and ionic degrees of freedom were performed with the following default VASP stopping criteria: EDIFF = $1{\cdot}10^{-6}$ eV, EDIFFG = $1{\cdot}10^{-5}$ eV. For calculations of the phonon frequencies and dielectric permittivity of the materials studied the stopping criteria were chosen to be two orders of magnitude smaller: EDIFF = $1{\cdot}10^{-8}$ eV, EDIFFG = $1{\cdot}10^{-7}$ eV. The dispersion of phonon bands and vibration density of states of a crystal were obtained by using the Phonopy post-process code [41,42].

Table 1 presents various parameters of $CdSe_{1-x}Te_x$ films and their corresponding substrates used in the experimental measurements. The film surfaces used for the reflectance measurements were of good quality, which allowed for mirror reflection mode with minimal surface scattering of the incident radiation in the far-infrared range. The size of polycrystalline grains in the thin layer was estimated by using the Debye-Sherrer equation, which involved measuring the width of the diffraction peaks

$$D = \frac{K\lambda}{\beta\cos\theta} \tag{1}$$

where $K = 0.9$ (shape dependent factor), and β is full width at half maximum (FWHM) of the dominant peak. The value D was determined similarly to in Refs. [43–45].

$$\rho = \frac{ZM}{N_a V} \tag{2}$$

where ρ – density, Z – number of atoms per unit cell ($Z = 4$ – for cubic crystal structure, $Z = 2$ – for hexagonal crystal structure), M – atomic weight ($M = M_{Cd} + (1 - x)M_{Se} + xM_{Te}$, x – from XRF), N_a – Avogadro's number, V – volume of the unit cell ($V = a^3$– for cubic crystal structure, $V = \frac{\sqrt{3}}{2}a^2c$– for cubic crystal structure).

The mean interatomic distance $d_{mean}^{(Cd-Se,\ Cd-Te)}$ is calculated using the known relation for the face-centered cubic structure (space group of symmetry no. 216),

$$d_{mean}^{(Cd\ -\ Se,Cd\ -\ Te)} = \frac{\sqrt{3}}{4}\sqrt[3]{V_c} = \frac{\sqrt{3}}{4}\sqrt[3]{\frac{(m^{(Cd)} + m^{(Se)} + m^{(Te)})}{\rho \cdot N_A}} \tag{3}$$

where V_c is unit cell volume, $(m^{(Cd)} + m^{(Se)} + m^{(Te)})$ is total unit cell mass, ρ is density and N_A is Avogadro number.

One can observe the expected opposite characters of the fitted linear dependences for the mean interatomic distance $d_{mean}^{(Cd-Te,\ Cd-Se)}$ and the density ρ on the content index $x^{(Te)}$ of the films studied (Fig. 3).

3. Experimental far-infrared spectra of $CdSe_{1-x}Te_x$ thin films

Only one distinct feature (maximum) of the experimental reflection spectrum $R(\lambda^{-1})$ is observed for CdSe (at about 170 cm^{-1}) and CdTe (at about 140 cm^{-1}) films (Fig. 4a). However, for $CdSe_{1-x}Te_x$ films, two reflectance features of $R(\lambda^{-1})$ with maxima at the wavenumbers close to those of CdSe and CdTe are detected in all three SSS compounds, $CdSe_{0.75}Te_{0.25}$, $CdSe_{0.5}Te_{0.5}$, and $CdSe_{0.25}Te_{0.75}$ (Fig. 4a). Similar two-mode behavior was observed in CdS_xSe_{1-x} thin films [46]. This result may confirm the assumption that the arrangement of atoms in the deposited $CdSe_{1-x}Te_x$ films studied is very close to the similar arrangements in the corresponding SSS. To verify this assumption, the

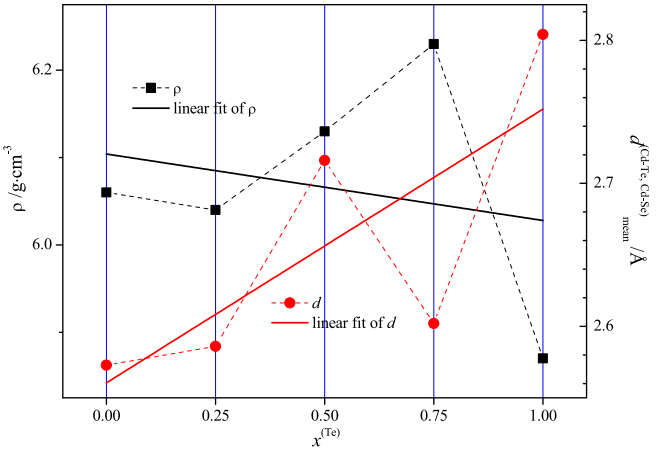

Fig. 3. Dependences of density ρ and mean interatomic distance $d_{mean}^{(Cd\text{-}Te,\ Cd\text{-}Se)}$ on the content index $x^{(Te)}$ for $CdSe_{1-x}Te_x$ films deposited by HF method (see Table 1).

Table 1
Parameters of $CdSe_{1-x}Te_x$ films and substrates.

Film on substrate	CdSe on quartz	CdTe on quartz	$CdSe_{0.5}Te_{0.5}$ on quartz	$CdSe_{0.5}Te_{0.5}$ on quartz	$CdSe_{0.25}Te_{0.75}$ on quartz	$CdSe_{0.75}Te_{0.25}$ on quartz
Deposition method*	HF	HF	QCV	HF	HF	HF
Substrate dimensions	~16 × 8 × 1.1 mm^3	~16 × 8 × 1.1 mm^3	14 (diameter) mm	~8 × 16 mm^2	~8 × 16 mm^2	~8 × 16 mm^2
Film thickness /μm	0.73	0.72	1.2	~1.2	~1.18	~0.89
Crystal structure	Cubic *F*-43 *m*	Cubic *F*-43 *m*	Cubic *F*-43 *m*	Cubic *F*-43 *m*	Hexagonal $P6_3/mmc$	Hexagonal $P6_3/mmc$
D, nm	89.8	45.3	53.82	51.3	50.9	34.9
ρ, g/cm^3 **	6.06	5.87	5.97	6.13	6.23	6.04
$d_{mean}^{(Cd\text{-}Se,\ Cd\text{-}Te)}$ /Å***	2.573	2.804	2.769	2.716	2.602	2.586

*HF – high-frequency magnetron sputtering (13.6 MHz); QCV – quasi-closed volume method.
** The density of the samples is calculated using the relation (2).

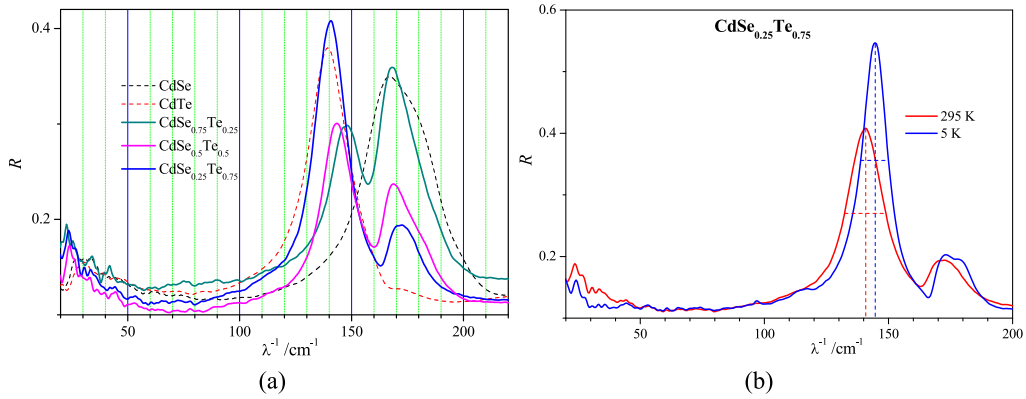

Fig. 4. Reflection spectra $R(\lambda^{-1})$ of (a) CdSe, CdTe, and $CdSe_{1-x}Te_x$ films deposited by HF method at the temperature 295 K and (b) $CdSe_{0.25}Te_{0.75}$ film at the temperatures 295 K and 5 K.

theoretical DFT calculations were carried out and the corresponding results are presented in the next subchapter.

No clear extrema in the reflection spectra $R(\lambda^{-1})$ of the studied samples were detected at room temperature in the range of 20 to 110 cm^{-1}. However, a relatively small decrease in the reflection coefficient R was observed in the range of 20 to 70 cm^{-1}. This decrease could be caused by the quasi-free electrons/holes due to the structural defects and/or remnant doping of $CdSe_{1-x}Te_x$ films. However, this possibility requires further separate study.

Fig. 4b depicts the changes in the reflection spectrum of $CdSe_{0.25}Te_{0.75}$ film as it is cooled down to 5 K. The changes observed are as expected, including a high-frequency shift, a decrease in the full width at half maximum (FWHM), and an increase in the maximum value of the reflection coefficient R. The high-frequency shift is caused by the decrease in the unit cell dimensions of the films as the temperature decreases. The decrease in FWHM with decreasing temperature is also a common feature of the phonon–phonon interaction.

4. Results of theoretical calculations of $CdSe_{1-x}Te_x$ SSS, comparison with experiment and discussion

The calculations were performed based on the cubic conventional 1 × 1 × 1 unit cell crystal structure of CdSe (Cd_4Se_4) and CdTe (Cd_4Te_4), space group of symmetry no. 216 (*F*-43 *m*). The equality of the supercell dimensions $a = b = c$ was kept also when the necessary optimizations of the atomic positions in the 2 × 2 × 2 supercells of CdSe-CdTe solid-state solutions ($Cd_{32}Se_{32(1-x)}Te_{32x}$, x = 0, 0.25, 0.5, 0.75, 1) were performed. For the thus obtained supercells $Cd_{32}Se_{32(1-x)}Te_{32x}$, the symmetries of the conventional 1 × 1 × 1 unit cell crystal structures of the SSS $CdSe_{0.75}Te_{0.25}$ and $CdSe_{0.25}Te_{0.75}$ are found to be cubic with the space group no. 215 (*P*-43 *m*), while the SSS $CdSe_{0.5}Te_{0.5}$ is characterized by the tetragonal group of symmetry of the space group no. 115 (*P*-4 *m*2). The crystals of SSS $CdSe_{1-x}Te_x$ were obtained by replacing the selenium with the tellurium atoms in the conventional unit cell Cd_4Se_4. Thus, the following crystal structures were obtained: CdSe, $CdSe_{0.75}Te_{0.25}$, $CdSe_{0.5}Te_{0.5}$ and $CdSe_{0.25}Te_{0.75}$, and CdTe. To avoid the interaction between the periodic images of atoms in the neighboring conventional unit cells the supercells 2 × 2 × 2 (64 atoms) with linear dimensions close to 12 Å were created for the DFT calculations using the VESTA code [47]. As a consequence of these crystal symmetries, all components of the dielectric permittivity tensor of cubic crystals (space groups no. 216 and no. 215) are equal, $\varepsilon_x = \varepsilon_y = \varepsilon_z$, when for crystals of the tetragonal symmetry (space group no. 115) the relation $\varepsilon_x = \varepsilon_y \neq \varepsilon_z$ takes place.

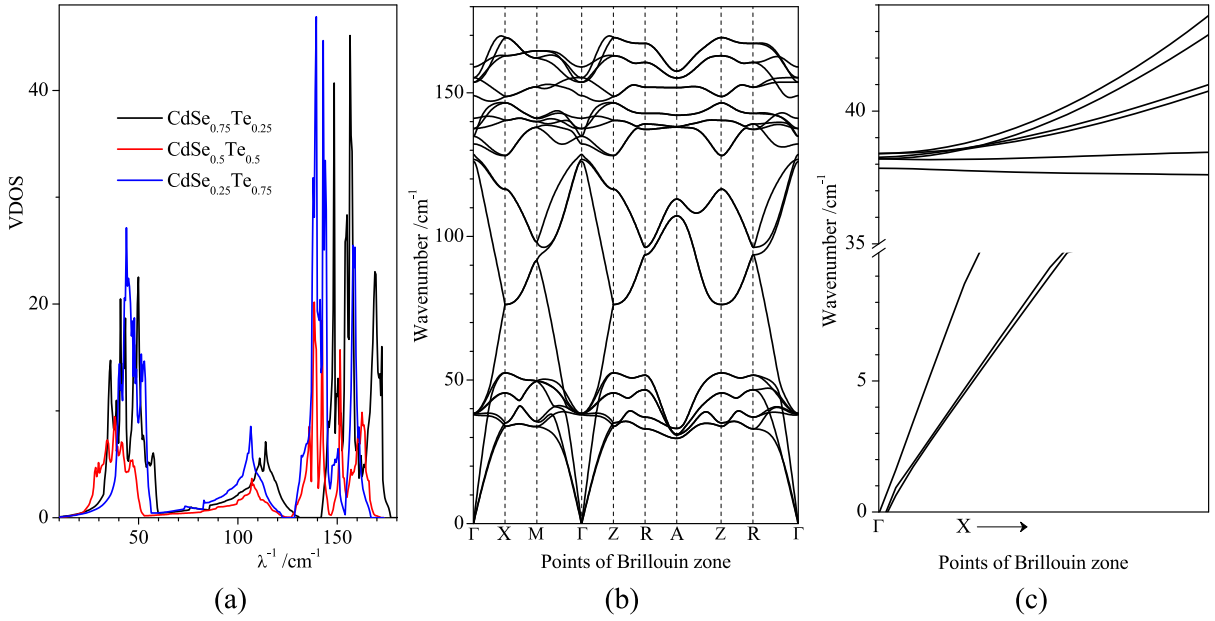

Fig. 5. Calculated at GGA-PE exchange-and-correlation functional and 2 × 2 × 2 supercells (a) the vibration density of states VDOS(λ^{-1}) for $CdSe_{0.75}Te_{0.25}$, $CdSe_{0.5}Te_{0.5}$, and $CdSe_{0.25}Te_{0.75}$ SSS and (b, c) the dispersions of phonon energy bands for $CdSe_{0.5}Te_{0.5}$ SSS.

The vibrational density of states (VDOS) of $CdSe_{0.75}Te_{0.25}$, $CdSe_{0.5}Te_{0.5}$ and $CdSe_{0.25}Te_{0.75}$ crystals calculated by using VASP and Phonopy codes are presented in Fig. 5a. The frequency range of 0 to 60 cm^{-1} corresponds to the acoustic and optical phonon modes, while the range of 90 to 190 cm^{-1} relates only to the optical phonon modes of the crystals. The VDOS median frequency in the range of 0 to 60 cm^{-1} is lowest for the mixed compound $CdSe_{0.5}Te_{0.5}$, compared to $CdSe_{0.75}Te_{0.25}$ and $CdSe_{0.25}Te_{0.75}$. This is likely due to the higher mass disorder in $CdSe_{0.5}Te_{0.5}$ compared to the other two crystals. This mass disorder could be the main reason for the lowest coefficient of thermal conductivity in semiconductor alloys [48].

The $CdSe_{0.5}Te_{0.5}$ material exhibits three acoustic and six optical phonon bands within the frequency range of 0 to 60 cm^{-1}. This means that the material is likely to absorb infrared radiation around the wavenumber of 40 cm^{-1}, which can only occur at the Brillouin zone's Γ-point. However, there is no band dispersion extremum at the Γ-point within the 90–120 cm^{-1} range, where the maximum of VDOS is observed (as shown in Fig. 5a). This indicates that the prediction of infrared absorption in this range is impossible. On the other hand, there are numerous band extrema within the Γ-point spectral range of 125–180 cm^{-1} (as shown in Fig. 5b), making infrared absorption in this range possible.

The graphs in Fig. 6 shows the vibration partial density of states (VPDOS) for $CdSe_{0.5}Te_{0.5}$, calculated using GGA-PE and GGA-PS exchange-and-correlation functionals. The VPDOS curves in Fig. 6a and b are similar, with the main difference being a slight shift of the VPDOS (λ^{-1}) curve calculated using GGA-PS to higher frequencies by about 10 cm^{-1}. This shift is caused by smaller unit cell volume (and unit cell dimensions) obtained within the Perdew–Burke–Ernzerhof pseudopotential for solids (PS) in comparison to the usual Perdew–Burke–Ernzerhof one (PE): the smaller crystal unit cell volume causes the higher the frequencies of phonon vibrations. In the low-frequency range of 0–130 cm^{-1}, the VPDOS values for Cd, Se, and Te are comparable, with Cd having a slightly higher VPDOS value. However, in the range of 130–180 cm^{-1} (as shown in Fig. 6a), there are significant changes in the VPDOS and optical absorption (as shown in Fig. 4a). Due to the smaller atomic mass of selenium ($M^{(Se)} = 78.97$) in comparison to tellurium ($M^{(Te)} = 127.60$), the largest VPDOS values of selenium are placed in the higher part of the range 130–180 cm^{-1} (Fig. 6a, b).

Experimental reflection spectra of CdSe and CdTe thin films show only one clear maximum in the range of 0 to 220 cm^{-1}, which corresponds to the phonon excitations. The positions of the calculated maxima of the dielectric functions $\varepsilon_2(\lambda^{-1})$ of CdSe and CdTe crystals are similar to the positions of the experimentally obtained reflection features $R(\lambda^{-1})$ of the corresponding thin films, as shown in Fig. 7. The calculated static dielectric permittivities (ionic contribution) of CdSe and CdTe crystals obtained using the GGA-PS exchange-and-correlation functional are $\varepsilon_1^{(CdSe)}(\lambda^{-1} = 0) = 3.38$ and $\varepsilon_1^{(CdTe)}(\lambda^{-1} = 0) = 2.88$, respectively. These values are in acceptable agreement with the corresponding reference values, which are 3.44 and 3.05, respectively [49].

It is expected that the frequency position of the highest point of the calculated dielectric function ($\varepsilon_2(\lambda^{-1})$) of crystals depends on the distance between the atoms. For example, in the case of CdTe, this distance is between cadmium and tellurium ions, indicated as d_{CdTe}. In thin films, the broad phonon features of the reflection spectra ($R(\lambda^{-1})$) can be caused by the dispersion of the corresponding interatomic distances. This claim is supported by the comparison of the experimental reflection spectrum $R(\lambda^{-1})$ and the calculated dielectric function ($\varepsilon_2(\lambda^{-1})$) of CdTe crystal (Fig. 7). The dispersion of the mean interatomic distances in CdSeTe thin films can be proportional to the surface-to-volume relation of the grains in the polycrystalline thin films because the near-surface interatomic distances are smaller than those deep in the body of the grain.

We conducted a study to examine the impact of surface on the interatomic distances between cadmium and tellurium surface atoms. To accomplish this, we performed the structure optimization of a CdTe slab in a supercell 12.8 Å × 12.8 Å × 27 Å. The supercell contained 64 atoms ($Cd_{32}Te_{32}$) of the initial supercell 12.8 Å × 12.8 Å × 12.8 Å at the cubic group of symmetry no. 216. For the limited structure optimization, we found that the distances between cadmium and tellurium atoms at the surface, $d_{surface1}^{(Cd-Te)}$ and $d_{surface2}^{(Cd-Te)}$, were 2.62 Å and 3.51 Å respectively. These distances were smaller and larger than the corresponding one $d^{(Cd-Te)}$, which was 2.88 Å for the bulk-like atoms. For the free structure optimization, the largest Cd-Te surface distance was found to be $d_S^{(Cd-Te)} = 4.05$ Å. This distance may be too large to create sufficiently strong interatomic bonds Cd-Te, thus one can expect the less strongly bonded cadmium atoms on the surface of polycrystalline CdTe grains. The value of this effect should be proportional to the surface-to-volume relation of CdTe grains. Consequently, one could expect the redshift of the strongest absorption maximum (at 139–140 cm^{-1} for bulk CdTe) for the thin films and relatively small polycrystalline grains of CdTe. The red frequency shifts in the Raman spectra of the free-standing CdSe nanocrystals were detected experimentally in Ref. [50].

Considering the relatively large characteristic grain dimension of the CdTe film studied, $D = 45.3$ nm (Table 1), no substantial changes are expected in the above-mentioned frequency of the transversal optical (TO) vibration mode of CdTe caused by the quantum confinement effect or by the attenuation of interatomic bonding of the surface ions due to the increased surface-to-volume relation. The latter reason may be justified by the relatively small relation of surface-to-volume number of atoms, $N_S/N_V = 0.007$, for CdTe polycrystalline grains of the dimension $D = 45.3$ nm (Table 1). Results of the reference study using Raman spectroscopy of CdSe nanoparticles [50] indicate changes in the phonon mode frequency $\Delta\lambda^{-1} = 5$ cm^{-1} for the grain dimension (D) changes between 3.9 to 5.6 nm. For the latter dimensions of the polycrystalline grains, the relation $N_S/N_V = 0.09$, which is one order of magnitude

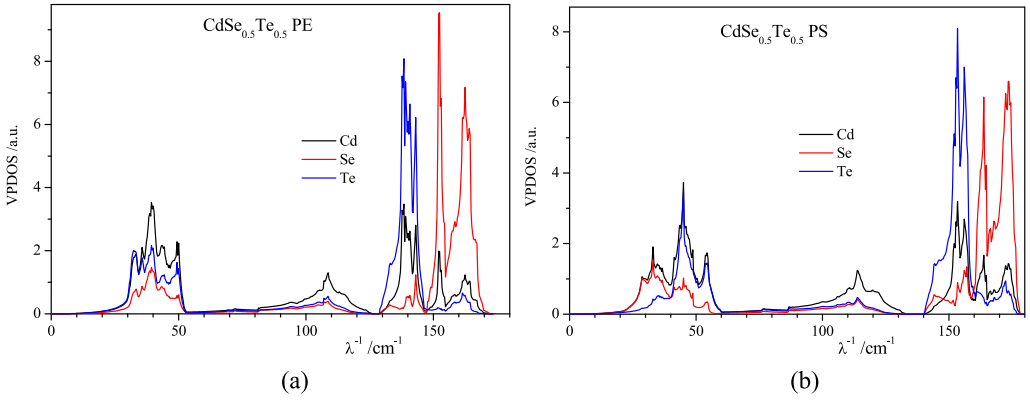

Fig. 6. (a) Calculated at (a) GGA-PE and (b) GGA-PS exchange-and-correlation functionals the spectra of the vibration partial density of states VPDOS(λ^{-1}) of $CdSe_{0.5}Te_{0.5}$ crystal.

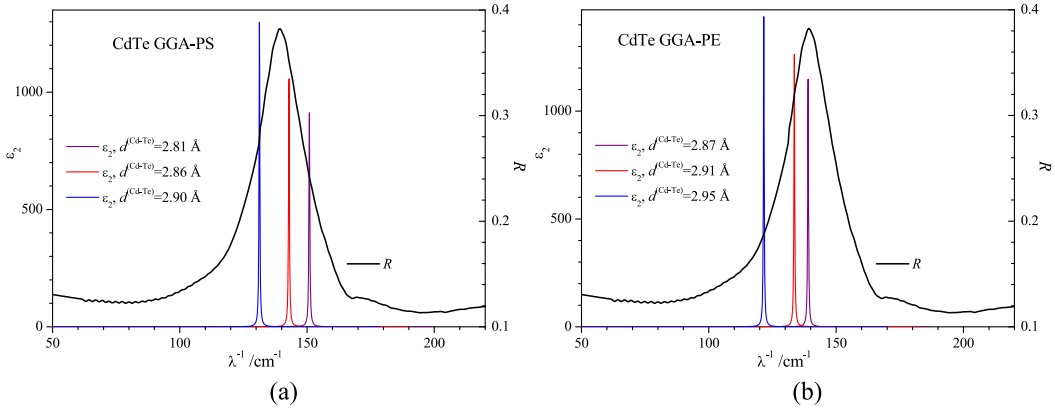

Fig. 7. Calculated spectrum of the imaginary part of dielectric function $\varepsilon_2(\lambda^{-1})$ of CdTe crystal at the cubic space group of symmetry no. 216 for (a) GGA-PS and (b) GGA-PE exchange-and-correlation functionals and the experimental spectrum of the normal incidence reflection coefficient $R(\lambda^{-1})$ of thin CdTe film ($d = 0.72$ μm).

larger than those for the studied CdTe thin films.

One can assume that the finite width of the experimental reflection maximum at the wavenumber of 139 cm^{-1} (Fig. 7) is caused by the dispersion of the interatomic distances due to the temperature vibrations of atoms. To verify this assumption, we conducted the DFT calculations of the NVE molecular dynamics of the CdTe crystal at 200 K for a duration of 10 ps. This was performed using the corresponding supercell 2 × 2 × 2 at the initial space group of symmetry no. 216, with the volume and total energy kept constant. We then calculated the dielectric function of CdTe for the atomic position set corresponding to the last step in the MD process, and compared it to the fitted dielectric function using one Lorentz function. The obtained fitted dielectric function and the corresponding FWHM (Fig. 8b) are similar to the experimental reflection spectrum obtained at the ambient temperature of 295 K (Fig. 4a). This result supports the assumption that the finite width of the experimental vibration maximum may be due to the deviations of the interatomic distances in CdTe thin film from one theoretical value corresponding to the temperature $T = 0$ and the space group of symmetry no. 216.

The calculated imaginary part of dielectric function $\varepsilon_2(\lambda^{-1})$ shows the detectable values in the ranges of 40–70 cm^{-1} (Fig. 8a). This can explain a presence of the gentle decrease of the experimental reflection coefficient $R(\lambda^{-1})$ in the range of 50–70 cm^{-1} (Fig. 7), which can be caused by the excitation of phonon modes in the ranges of 40–70 cm^{-1} at finite temperatures, $T > 0$. In such case, the absorption of the far-infrared radiation by the free charge carriers (electrons or holes) is not necessary to explain this decrease of the experimental reflection coefficient $R(\lambda^{-1})$ in the range of 50–70 cm^{-1}.

The imaginary part of dielectric function ($\varepsilon_2(\lambda^{-1})$) and infrared intensity ($I_{norm}(\lambda^{-1})$) of $CdSe_{1-x}Te_x$ SSS show maximum values around the frequency range of 130–180 cm^{-1} (Fig. 9). The Born effective charges calculated by the VASP code were used to obtain the spectra of infrared intensity $I_{norm}(\lambda^{-1})$ using an additional algorithm called plotIR [51]. This algorithm calculates the peak intensity proportional to the Born effective charges and adds a Lorentzian smearing, resulting in a spectrum that can be compared with the experimental reflection and absorption spectra of the material. The DFT calculations ($\varepsilon_2(\lambda^{-1})$, $I_{norm}(\lambda^{-1})$, and eigenvectors of the dynamical matrix) were obtained using GGA-PS exchange-and-correlation functional. When using the GGA-PE exchange-and-correlation functional, similar dependencies of $\varepsilon_2(\lambda^{-1})$ and $I_{norm}(\lambda^{-1})$ are obtained, but they are shifted towards the range of smaller wavenumbers (λ^{-1}) (see the explanation corresponding to similar differences in VPDOS in Fig. 6).

Only one spectral peak is observed for CdSe and CdTe compositions. This is caused by the high cubic symmetry of the corresponding supercells and only one type of ionic bonding, either Cd – Se or Cd – Te. The spectral positions of maximum the imaginary part of dielectric function $\varepsilon_2(\lambda^{-1})$ obtained from our calculations for CdSe (167.6 cm^{-1}) and CdTe (141.4 cm^{-1}) crystals (Fig. 9) are in an expected inverse relation with the masses of Se ($M_{Se} = 78.9$) and Te ($M_{Te} = 127.6$) anion atoms and in good agreement with the experimentally observed reflection bands (Fig. 4).

Table 2 shows the positions of maxima in the experimental reflection spectra $R(\lambda^{-1})$ and in the computational spectra of the imaginary part of the dielectric function $\varepsilon_2(\lambda^{-1})$ of $CdSe_{1-x}Te_x$ SSS. The corresponding wavenumbers are in relatively good agreement.

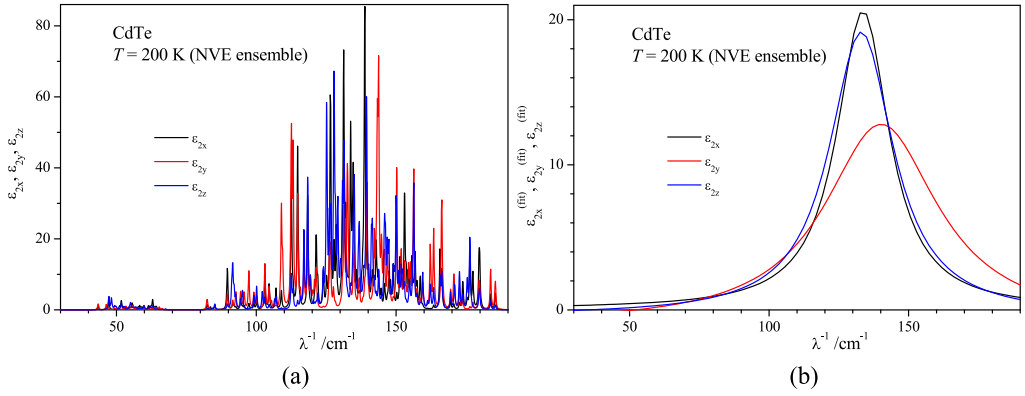

Fig. 8. Imaginary parts of dielectric function $\varepsilon_{2x}(\lambda^{-1})$, $\varepsilon_{2y}(\lambda^{-1})$, and $\varepsilon_{2z}(\lambda^{-1})$ of CdTe crystal (space group of symmetry no. 216, supercell 2 × 2 × 2) calculated for one of the atomic position sets of the molecular dynamics (NVE ensemble, temperature 200 K, duration of molecular dynamics 10 ps): (a) without additional treatment, (b) fitted by one Lorentz function.

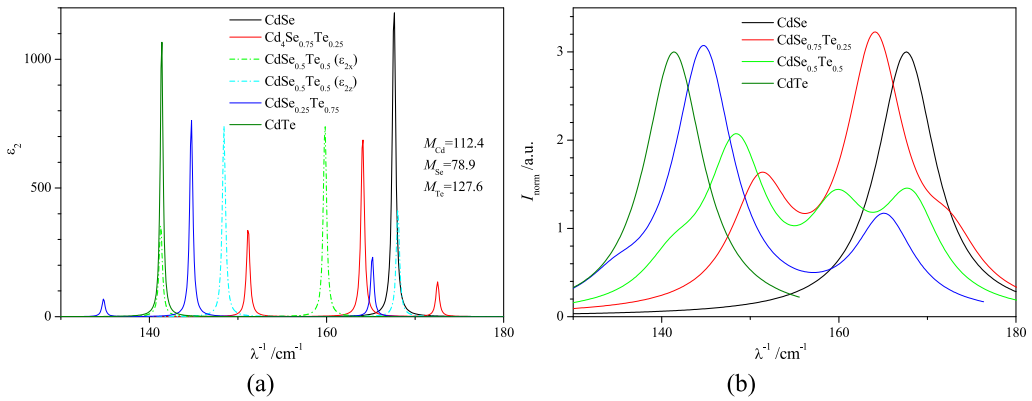

Fig. 9. Calculated spectra of (a) imaginary part of dielectric permittivity $\varepsilon_2(\lambda^{-1})$ and (b) normalized intensity $I_{norm}(\lambda^{-1})$ in the range of far-infrared absorption of $CdSe_{1-x}Te_x$ SSS for $x = 0$, 0.25, 0.5, 0.75, and 1.0 at $1 \times 1 \times 1$ supercells.

Table 2
Wavenumbers of maxima in the calculated spectra of the imaginary part of dielectric function $\varepsilon_2(\lambda^{-1})$ and experimental far-infrared reflection spectra $R(\lambda^{-1})$ of $CdSe_{1-x}Te_x$ SSS.

Solid state solution	Calculated wavenumbers for $\varepsilon_{2x} = \varepsilon_{2y}$ cm^{-1}	Calculated wavenumbers for ε_{2z} cm^{-1}	Experimental wavenumbers for R cm^{-1}
CdSe	167.6	167.6	167.2
$CdSe_{0.75}Te_{0.25}$	151.1; 164.1; 172.5	151.1; 164.1; 172.5	140.5; 172.3
$CdSe_{0.5}Te_{0.5}$	141.2; 159.8	148.4;168	143.4; 168.7; 180.6
$CdSe_{0.25}Te_{0.75}$	134.8; 144.7; 165.1	134.8; 144.7; 165.1	147.7; 168.1
CdTe	141.4	141.4	139.2

Fig. 10 shows the eigenvectors of three infrared vibration modes of the CdTe crystal. For each infrared mode (73, 74, and 75), the vibration eigenvectors/ion displacements (Δ_x, Δ_y, and Δ_z), are opposite in phases for cadmium and tellurium ions. This agrees with the expected change of electrical dipoles of Cd-Te ionic bonding upon absorption of infrared radiation.

Three spectral maxima of the dielectric function $\varepsilon_2(\lambda^{-1})$ have been observed in $CdSe_{1-x}Te_x$ SSS samples for $x = 0.25$ and $x = 0.75$ (as shown in Fig. 9), corresponding to different vibration modes. For $CdSe_{0.75}Te_{0.25}$, the ion displacements Δ are presented in Fig. 11, corresponding to the aforementioned three spectral maxima of $\varepsilon_2(\lambda^{-1})$. The characteristic feature of the vibration mode 89 (wavenumber 151.1 cm^{-1}) is the largest eigenvector for the heaviest tellurium ions, $M_{Te} = 127.6$, (the ion numbers 56–64) (as depicted in Fig. 11c). Conversely, the high-frequency mode 35 of wavenumber 172.5 cm^{-1} is realized due to the large displacement of the lighter selenium ions, $M_{Se} = 78.9$, (the ion numbers 48–56) (as shown in Fig. 11a). The middle-frequency vibration mode 65 (wavenumber 164.08 cm-1) is characterized by the relatively large eigenvectors for all selenium ions (as illustrated in Fig. 11b).

Similar features are observed for the dependence of the displacements Δ_x, Δ_y, and Δ_z of selenium and tellurium ions in the compound $CdSe_{0.25}Te_{0.75}$ (Fig. 12). The largest displacement Δ is observed for selenium ions when the wavenumber is $\lambda^{-1} = 165.16$ cm^{-1} (Fig. 12a). At smaller wavenumbers, 144.72 cm^{-1} and 134.81 cm^{-1}, the displacements of tellurium atoms become larger than those of selenium ones (Fig. 12b, c).

It is worth noting that in the case of selenium and tellurium ions discussed in the Figs. 10 to 12, their displacements in the x, y, and z directions are accompanied by opposite sign displacements of cadmium ions (from ion numbers 1 to 32) in the same polarization direction. This is a necessary condition for the crystal to absorb infrared radiation with the participation of the mentioned ion displacements.

The wavevectors corresponding to the maxima of the dielectric function $\varepsilon_{2x}(\lambda^{-1})$ at 159.82 cm^{-1} and 141.26 cm^{-1}, and $\varepsilon_{2z}(\lambda^{-1})$ at 168.05 cm^{-1}, 148.41 cm^{-1}, and 148.4 cm^{-1} of the content $CdSe_{0.5}Te_{0.5}$ (Fig. 9) are presented in Fig. 13.

An analysis of the wavevectors of the optical phonon modes, which correspond to the frequencies near 40 cm^{-1} (as shown in Fig. 5a and 6), has been conducted. It was found that, at the Γ-point of the Brillouin zone, the infrared absorption was absent ($\varepsilon_2 = 0$). This indicated that the summary displacements for cadmium, selenium, and tellurium ions in the crystal supercells were also absent, $\sum_i \Delta_i^{(Cd)} = \sum_i \Delta_i^{(Se)} = \sum_i \Delta_i^{(Te)} = 0$. Therefore, there was no dipole moment and infrared absorption in $CdSe_{1-x}Te_x$ when taken at cubic space groups of symmetry no. 216, no. 215, and tetragonal group no. 115. However, if the local symmetry of a certain atom environment decreased due to chaotic thermal vibrations

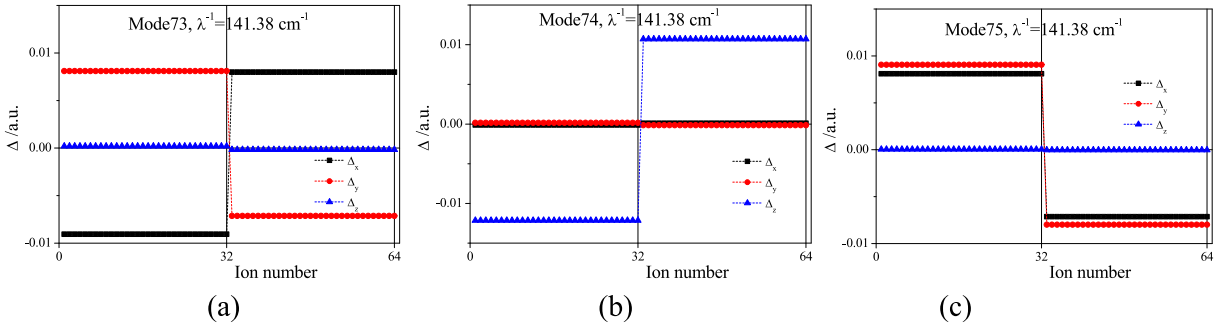

Fig. 10. Eigenvectors Δ_x, Δ_y, Δ_z of infrared vibration modes 73 (a), 74 (b), and 75 (c) corresponding to the maxima of the dielectric function $\varepsilon_2(\lambda^{-1})$ at 141.38 $cm^{-1}$of the content CdTe (olive line in Fig. 9). The ion numbers 1–32, 33–64 correspond to cadmium and tellurium ions, respectively.

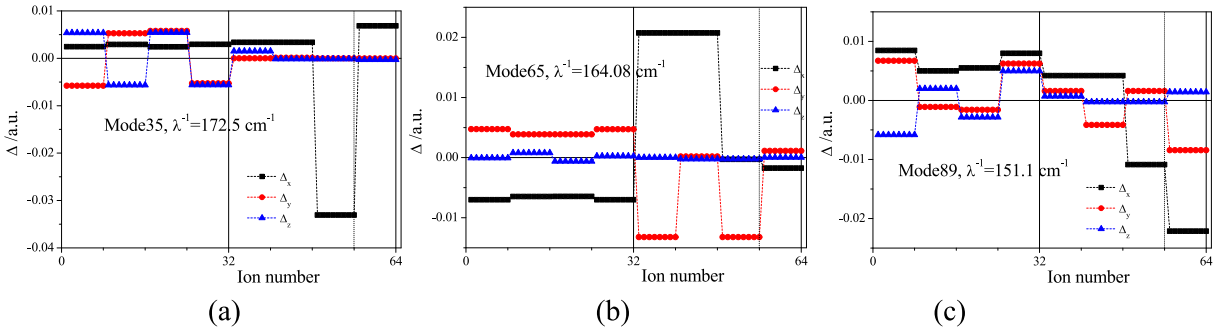

Fig. 11. Eigenvectors Δ_x, Δ_y, Δ_z of infrared vibration modes 35 (a), 65 (b), and 89 (c) corresponding to the maxima of the dielectric function $\varepsilon_2(\lambda^{-1})$ at 172.5 cm^{-1}, 164.08 cm^{-1}, and 151.1 cm^{-1} of the content $CdSe_{0.75}Te_{0.25}$ (red line in Fig. 9). The ion numbers 1–32, 33–56, and 57–64 correspond to cadmium, selenium, and tellurium ions, respectively. (For interpretation of the references to colour in this figure legend, the reader is referred to the web version of this article.)

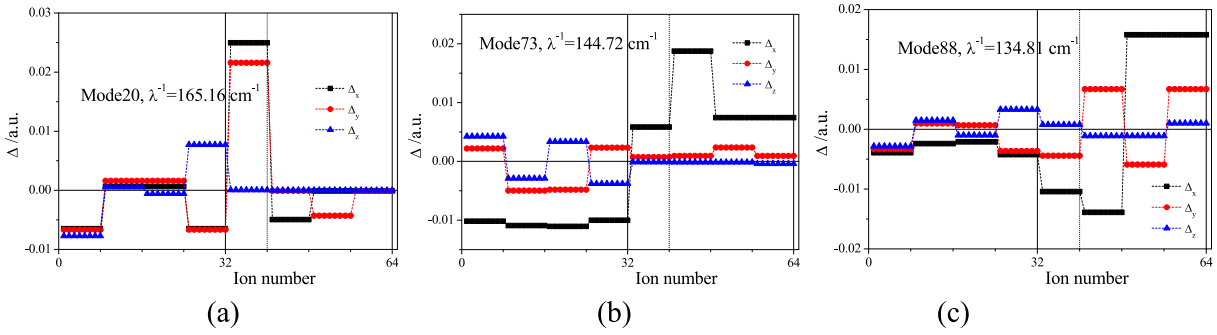

Fig. 12. Eigenvectors Δ_x, Δ_y, Δ_z of infrared vibration modes 20 (a), 73 (b), and 88 (c) corresponding to the maxima of the dielectric function $\varepsilon_2(\lambda^{-1})$ at 165.16 cm^{-1}, 144.72 cm^{-1}, and 134.81 cm^{-1} of the content $CdSe_{0.25}Te_{0.75}$ (blue line in Fig. 7). The ion numbers 1–32, 33–40, and 41–64 correspond to cadmium, selenium, and tellurium ions, respectively. (For interpretation of the references to colour in this figure legend, the reader is referred to the web version of this article.)

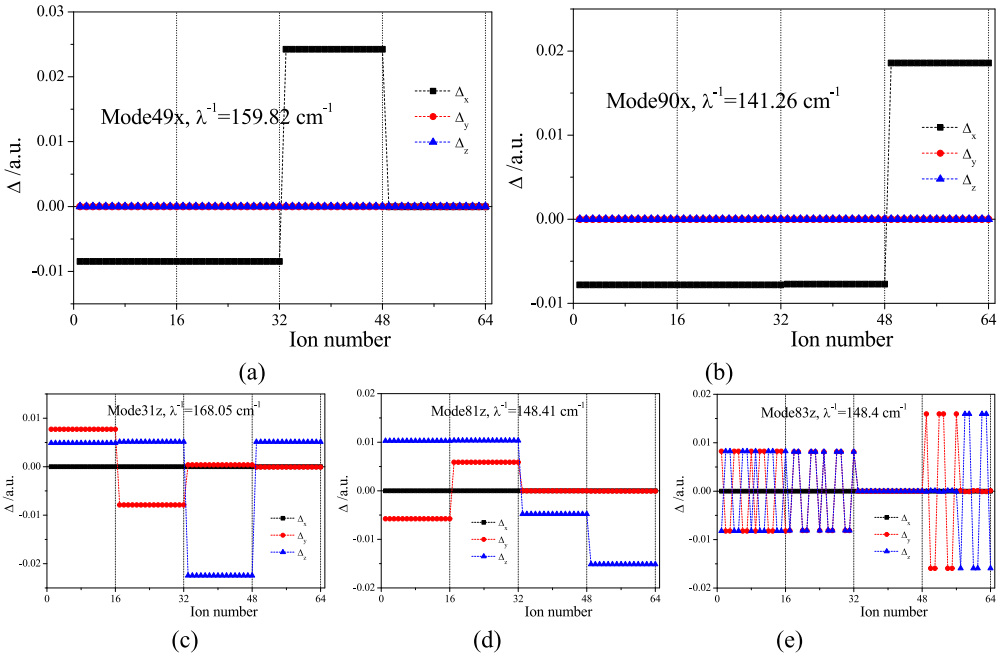

Fig. 13. Eigenvectors Δ_x, Δ_y, Δ_z of infrared vibration modes 49_x (a), 90_x (b), 31_z (c), 81_z (d), 83_z (e) corresponding to the maxima of the dielectric function $\varepsilon_{2x}(\lambda^{-1})$ at 159.82 cm^{-1} and 141.26 cm^{-1}, and $\varepsilon_{2z}(\lambda^{-1})$ at 168.05 cm^{-1}, 148.41 cm^{-1}, and 148.4 cm^{-1} of the content $CdSe_{0.5}Te_{0.5}$ (green and cyan lines in Fig. 9). The ion numbers 1–32, 33–48, and 49–64 correspond to cadmium, selenium, and tellurium ions, respectively. (For interpretation of the references to colour in this figure legend, the reader is referred to the web version of this article.)

of surrounded atoms, the corresponding summary dipole moment of this local structure may increase. This event leads to the increase of the infrared absorption, which means a nonzero imaginary part of the dielectric permittivity $\varepsilon_2 \neq 0$. This phenomenon is observed in the wavenumber range 40 cm^{-1} to 70 cm^{-1} for CdTe crystal at the simulated MD temperature of 200 K (as shown in Fig. 8a).

We conducted molecular dynamics to study the impact of polycrystalline grain dimensions of CdTe on the interatomic distances $d_{Cd\text{-}Te}$ and the frequencies of phonon maxima. The simulations were carried out at 50 K, NPT ensemble, and GGA-PE exchange-and-correlation functional for a thin CdTe slab, $Cd_{108}Te_{108}$, with a surface-to-volume number of atoms relation $N_S/N_V = 0.2$. It is worth noting that DFT computations of slabs are less demanding than those for quantum dots. The N_S/N_V value 0.2 used in our study is higher than the N_S/N_V value of CdSe polycrystalline grains with dimensions of 4–5.5 nm, which was estimated as 0.09 [50].

The frequency dependences of vibration density of states were obtained for CdTe single crystal (Fig. 14a). The maxima of these frequency dependences are in good agreement with the experimental value of the reflection spectrum (Fig. 4a). In Fig. 14a, the maxima of partial VDOS for Cd and Te and VDOS for CdTe occur at almost the same wavenumber λ^{-1}. The corresponding interatomic distance is $d_{Cd\text{-}Te} = 0.278$ nm, as shown in Fig. 14c.

The frequencies of maxima of VDOS dependences obtained for $Cd_{108}Te_{108}$ slab are smaller than those for CdTe single crystal. Moreover, the frequency of the partial VDOS maximum for Cd ions is smaller than that for Te ones. This suggests that the near-surface cadmium ions have weaker bonding with the tellurium ones than the near-surface tellurium ions with the cadmium ones. These results align with the previously stated findings of static structure optimization of CdTe slab in the supercell 12.8 Å×12.8 Å×27 Å containing 64 atoms ($Cd_{32}Te_{32}$), where the increased distances of the surface cadmium ions $d_{surface}^{(Cd-Te)} = 3.51$ Å and $d_{surface}^{(Cd-Te)} = 4.05$ Å were found. Therefore, it can be concluded that cadmium surface ions of CdTe thin slabs of the surface-to-volume number of atoms relation $N_S/N_V = 0.42$ are bonded to the surface tellurium ones weaker than the corresponding tellurium ions to cadmium ones. This may be due to the smaller ionic charge of cadmium surface ions in comparison to the corresponding bulk ones, despite the high ionic character of CdTe interatomic bonding, calculated based on the electronegativity of Cd and Te, which is relatively high, IC = 0.88. As a result, the ionic type interaction of the surface cadmium ions with tellurium ones may decrease.

It is interesting to note that the interatomic distance ($d_{(Cd\text{-}Te)}$) in CdTe thin slabs (about 0.270 nm) is less than that in the bulk of CdTe single crystal (approximately 0.278 nm) as shown in Fig. 14c. This difference in distance could result in the confinement effect in the electronic spectra of CdTe thin slabs. It is an area that can be explored in future studies.

The results shown in Fig. 14a and b are consistent with the experimentally observed redshift of the far-infrared absorption peak depicted in Fig. 2.

5. Conclusions

Comprehensive experimental and theoretical investigations were carried out to study the far-infrared spectra of $CdSe_{1-x}Te_x$ films deposited on quartz substrates. The reflection spectra of $CdSe_{1-x}Te_x$ films with varying compositions ($x = 0$, 0.25, 0.5, 0.75, and 1.0) were compared with the corresponding theoretical spectra obtained for the cubic space groups of symmetry *F*-43 *m* (CdSe, CdTe), *P*-43 *m* ($CdSe_{0.75}Te_{0.25}$, $CdSe_{0.25}Te_{0.75}$), and the tetragonal group *P*-4 *m*2 ($CdSe_{0.5}Te_{0.5}$). The experimental and theoretical results were found to be in excellent agreement.

The phonon band structures and vibration densities of $CdSe_{1-x}Te_x$ solid state solutions have been calculated and categorized into three frequency ranges: 0–60 cm^{-1}, 60–130 cm^{-1}, and 130–180 cm^{-1}. It has been observed that only the last range is infrared active. This conclusion was drawn after carefully analyzing the eigenvectors of the dynamical matrices of the compound studied.

Through additional DFT calculations, it was shown that the increased widths of maxima in the reflection spectra of the deposited $CdSe_{1-x}Te_x$ films studied may be caused by the different interatomic distances $d^{(Cd\text{-}Se/Te)}$ due to the dispersion in the grain size dimensions of the polycrystalline films. Furthermore, the FWHM of only one experimental reflectance phonon maximum of CdTe was found to be similar to the FWHM of the fitted dielectric function $\varepsilon_2(\lambda^{-1})$ obtained by the DFT-based MD of the crystal at the temperature of 200 K.

Within the wavenumber range of 50–70 cm^{-1} and 80–120 cm^{-1}, the reflection spectra of $CdSe_{1-x}Te_x$ films exhibit gentle features that are caused by the activation of phonon modes at finite temperatures ($T > 0$). The intensities of these modes are proportional to the temperature. However, they do not provide sufficient evidence for the presence of free charge carriers in the sample being studied. It is more likely that the gentle decrease of the reflective coefficient $R(\lambda^{-1})$ in the range 50–70 cm^{-1} is not due to the possible quasi-free charge carriers (electrons or holes).

Taking into account the relatively large polycrystalline grain dimensions of $CdSe_{1-x}Te_x$ films studied ($D \approx 50$ nm), the influence of the size effects on the spectral position of maxima in the far-infrared absorption spectra is rather negligible.

It was discovered that the maximum of the MD vibration density of states of $Cd_{108}Te_{108}$ thin slab caused a redshift in comparison to the far-infrared absorption mode of CdTe single crystal. This redshift is quite significant ($\approx$ 30 cm^{-1}) due to the fact that the thin slab has a large surface-to-volume ratio of $N_S/N_V = 0.2$. For the $Cd_{108}Te_{108}$ thin slab and CdTe single crystal, the mean interatomic distances are respectively equal to $d_{Cd\text{-}Te} \approx 0.270$ nm and $d_{Cd\text{-}Te} \approx 0.278$ nm, which suggests that the CdTe thin slab substance is compressed.

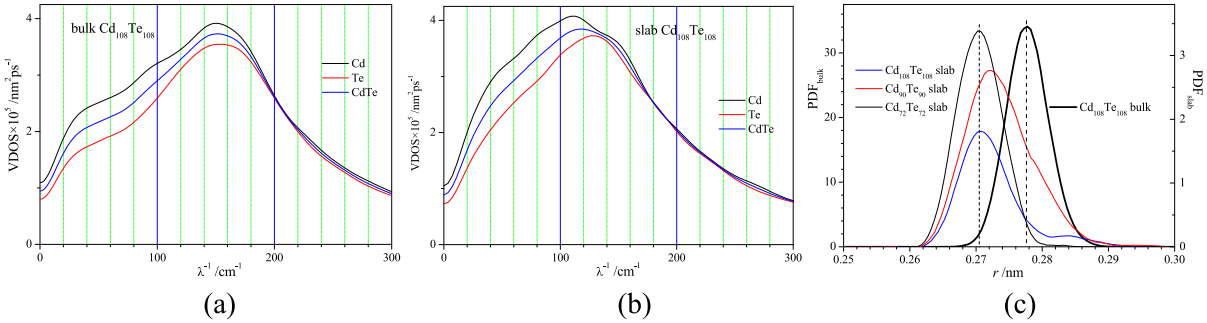

Fig. 14. Vibrational density of states (VDOS) of (a) single crystal (supercell 3 × 3 × 3, $N_{at} = 216$) and (b) corresponding slab perpendicular to *z*-axis and (c) pair distribution functions (PDF) for CdTe single crystal and slabs $Cd_{108}Te_{108}$, $Cd_{90}Te_{90}$, and $Cd_{72}Te_{72}$ of different numbers of atoms. All results relate to the MD temperature of 50 K at NPT ensemble.

CRediT authorship contribution statement

Andrii I. Kashuba: Writing – original draft, Validation, Software, Methodology, Investigation, Data curation. **Leszek Bychto:** Visualization, Resources, Methodology, Investigation, Data curation. **Krzysztof Dorywalski:** Writing – review & editing, Visualization, Resources, Investigation, Formal analysis, Data curation. **Roman Petrus:** Visualization, Validation, Methodology, Investigation, Formal analysis. **Alexander Veber:** Visualization, Resources, Project administration, Methodology, Investigation, Formal analysis, Data curation. **Ljiljana Puskar:** Visualization, Resources, Project administration, Methodology, Investigation, Formal analysis, Data curation. **Ulrich Schade:** Writing – original draft, Visualization, Validation, Resources, Project administration, Methodology, Investigation, Formal analysis, Data curation. **Ihor V. Semkiv:** Resources, Methodology, Investigation, Data curation. **Bohdan Andriyevsky:** Writing – review & editing, Writing – original draft, Visualization, Validation, Supervision, Software, Project administration, Methodology, Investigation, Conceptualization.

Declaration of competing interest

The authors declare that they have no known competing financial interests or personal relationships that could have appeared to influence the work reported in this paper.

Data availability

Data will be made available on request.

Acknowledgements

Experimental measurements with using the synchrotron radiation of BESSY II operated by the Helmholtz-Zentrum Berlin für Materialien und Energie were performed in the framework of the BESSY proposal 221-10763-ST. Computer calculations were performed at ICM of Warsaw University, Poland (projects No. g86-1023, 89-1293 and g93-1636) and WCSS of the Wrocław University of Technology, Poland (project No. 053).

References

[1] S. Philipps, W. Warmuth, Photovoltaics Report. Fraunhofer ISE: Freiburg, Germany, 2019.
[2] M.A. Green, E.D. Dunlop, D.H. Levi, J. Hohl-Ebinger, M. Yoshita, A.W.Y. Ho-Baillie, Prog. Photovolt. Res. Appl. 27 (2019) 565–575.
[3] First Solar Press Release, First Solar Achieves Yet another Cell Conversion Efficiency World Record; First Solar Press Release: Tempe, AZ, USA, 2016.
[4] T. Ablekim, J.N. Duenow, X. Zheng, H. Moutinho, J. Moseley, C.L. Perkins, S. W. Johnston, P.O. Keefe, E. Colegrove, D.S. Albin, M.O. Reese, W.K. Metzger, ACS Energy Lett. 5 (2020) 892–896.
[5] A.H. Munshi, J. Kephart, A. Abbas, J. Raguse, J.N. Beaudry, K. Barth, J. Sites, J. Walls, W. Sampath, IEEE J. Photovolt. 8 (2018) 310–314.
[6] A.M. Bothwell, J.A. Drayton, P.M. Jundt, J.R. Sites, MRS Adv. 4 (2019) 2053–2062.
[7] R.M. Geisthardt, M. Topič, J.R. Sites, IEEE J. Photovolt. 5 (2015) 1217–1221.
[8] N. Muthukumarasamy, S. Jayakumar, M.D. Kannan, R. Balasundaraprabhu, Sol. Energy 83 (2009) 522–526.
[9] D.E. Swanson, J.R. Sites, W.S. Sampath, Sol. Energy Mater. Sol. Cells 159 (2017) 389–394.
[10] T. Wang, S. Ren, C. Li, W. Li, C. Liu, J. Zhang, L. Wu, B. Li, G. Zeng, Sol. Energy 164 (2018) 180–186.
[11] T.A.M. Fiducia, B.G. Mendis, K. Li, C.R.M. Grovenor, A.H. Munshi, K. Barth, W. S. Sampath, L.D. Wright, A. Abbas, J.K. Bowers, J.M. Walls, Nat. Energy 4 (2019) 504–511.
[12] J.D. Poplawsky, W. Guo, N. Paudel, A. Ng, K. More, D. Leonard, Y. Yan, Nat. Commun. 7 (2016), 12537 (1–9).
[13] L. Kumar, B.P. Singh, A. Misra, S. Misra, T. Sharma, Phys. B Condens. Matter 363 (2005) 102–109.
[14] T.C.M. Santhosh, K.V. Bangera, G.K. Shivakumar, Sol. Energy 153 (2017) 343–347.
[15] A.J. Strauss, J. Steininger, J. Electrochem. Soc. 117 (1970) 1420–1426.
[16] N. Muthukumarasamy, R. Balasundaraprabhu, S. Jayakumar, M.D. Kannan, Mater. Sci. Semicon. Proc. 102 (2007) 86–91.
[17] D. Ravichandran, F.P. Xavier, S. Sasikala, S.M. Babu, Bull. Mater. Sci. 19 (1996) 437–442.
[18] M. Lingg, A. Spescha, S.G. Haass, R. Carron, S. Buecheler, A.N. Tiwari, Sci. Technol. Adv. Mater. 19 (2018) 683–692.
[19] N. Muthukumarasamy, R. Balasundaraprabhu, S. Jayakumar, M.D. Kannan, Sol. Energy Mater. Sol. Cells 92 (2008) 851–856.
[20] D.N. Talwar, T.-R. Yang, Z.C. Feng, P. Becla, Infrared reflectance and transmission spectra in II-VI alloys and superlattices, Phys. Rev. B 84 (2011) 174203–174211.
[21] M.M. Ivashchenko, A.S. Opanasyuk, V.I. Perekrestov, V.V. Kosyak, Y.P. Gnatenko, V.M. Kolomiets, Morphological, structural, compositional properties and IR-spectroscopy of CdSe films deposited by close-spaced vacuum sublimation, Vacuum 119 (2015) 81–87.
[22] A.I. Kashuba, B. Andriyevsky, I.V. Semkiv, H.A. Ilchuk, R.Y. Petrus, S. V. Shyshkovskyi, Calculation of the vibrational spectra of CdSe and CdS crystals with zinc blende structure, Mater. Today: Proc. 62 (2022) 5812–5818.
[23] A.I. Lebedev, B.M. Saidzhonov, K.A. Drozdov, A.A. Khomich, R.B. Vasiliev, Raman and infrared studies of CdSe/CdS core/shell nanoplatelets, J. Phys. Chem. C 125 (2021) 6758–6766.
[24] Akhilesh K. Arora, M. Rajalakshmi, T. R. Ravindran, Phonon confinement in nanostructured materials. *Encyclopedia of Nanoscience and Nanotechnology*, Ed. by H. S. Nalwa, **8** (2004) 499–512.
[25] *Semiconductors*, edited by O. Madelung, W. von der Osten, U. Rössler, Springer, Berlin, 1982, Landolt-Burstein, New Series, Group III, Vol. 22a.
[26] A.V. Baranov, Y.P. Rakovich, J.F. Donegan, T.S. Perova, R.A. Moore, D.V. Talapin, A.L. Rogach, Y. Masumoto, I. Nabiev, Effect of ZnS shell thickness on the phonon spectra in CdSe quantum dots, Phys. Rev. B 68 (2003) 165306.
[27] M.A. Hines, P. Guyot-Sionnest, J. Phys. Chem. 110 (1996) 468.
[28] J.-Yu. Zhang, X.-Y. Wang, M. Xiao, L. Qu, X. Peng, *Appl. Phys. Lett.* **81** (2002) 2076.
[29] B. Andriyevsky, L. Bychto, K. Dorywalski, U. Schade, L. Puskar, A. Patryn, A. Hapka, K. Mydłowska, A. Veber, A.I. Kashuba, K.T.R. Reddy, The optical properties of In_2S_3 films in the far-infrared spectral range, Infrared Phys Techn 131 (2023) 104662.
[30] U. Schade, M. Ortolani, J. Lee, THz experiments with coherent synchrotron radiation from BESSY II, Synchrotron Radiation News 20 (2007) 17–24.
[31] E.J. Danielewicz, P.D. Coleman, Far infrared optical properties of selenium and cadmium telluride, Appl. Opt. 13 (5) (1974) 1164.
[32] H. Wolter, Optik dünner Schichten, in: S. Flügge (Ed.), Grundlagen Der Optik, Springer-Verlag, Berlin, 1956, pp. 461–554.
[33] G. Kresse, J. Hafner, Ab initio molecular dynamics for liquid metals, Phys. Rev. B 47 (1993) 558–561.
[34] G. Kresse, J. Hafner, Ab initio molecular-dynamics simulation of the liquid-metal-amorphous-semiconductor transition in germanium, Phys. Rev. B 49 (1994) 14251–14269.
[35] G. Kresse, J. Furthmüller, Efficiency of ab-initio total energy calculations for metals and semiconductors using a plane-wave basis set, Comput. Mater. Sci. 6 (1996) 15–50.
[36] G. Kresse, J. Furthmüller, Efficient iterative schemes for ab initio total-energy calculations using a plane-wave basis set, Phys. Rev. B 54 (1996) 11169–11186.
[37] P.E. Blöchl, Projector augmented-wave method, Phys. Rev. B 50 (1994) 17953–17979.
[38] G. Kresse, D. Joubert, From ultrasoft pseudopotentials to the projector augmented-wave method, Phys. Rev. B 59 (1999) 1758–1775.
[39] J.P. Perdew, A. Ruzsinszky, G.I. Csonka, O.A. Vydrov, G.E. Scuseria, L. A. Constantin, X. Zhou, K. Burke, Restoring the density-gradient expansion for exchange in solids and surfaces, Phys. Rev. Lett. 100 (2008) 136406.
[40] M. Methfessel, A.T. Paxton, High-precision sampling for Brillouin-zone integration in metals, Phys. Rev. B 40 (1989) 3616–3621.
[41] A. Togo, L. Chaput, T. Tadano, I. Tanaka, Implementation strategies in phonopy and phono3py, J. Phys. Condens. Matter 35 (2023) 353001-1–353022.
[42] A. Togo, First-principles phonon calculations with Phonopy and Phono3py, J. Phys. Soc. Jpn. 92 (2023) 012001-1–012021.
[43] A.I. Kashuba, B. Andriyevsky, Growth and crystal structure of $CdTe_{1-x}Se_x$ ($x \geq 0.75$) thin films prepared by the method of high-frequency magnetron sputtering, Low Temp. Phys. 50 (1) (2024) 32–36.
[44] A.I. Kashuba, H.A. Ilchuk, I.V. Semkiv, B. Andriyevsky, Y.M. Storozhuk, R.Y. Petrus, Optical properties of CdSe thin films with different thicknesses obtained by the method of high-frequency magnetron sputtering, Roman. J. Phys. **68**(5–6) (2023) 204(17).
[45] H.A. Ilchuk, R.Y. Petrus, A.I. Kashuba, I.V. Semkiv, E.O. Zmiyovska, Optical-energy properties of the bulk and thin-film cadmium telluride (CdTe), Nanosistemi, Nanomateriali, Nanotehnologii. 16 (3) (2018) 519–533.
[46] W.S.O. Rodden, C.M.S. Torres, C.N. Ironside, Semicond. Sci. Technol. 10 (1995) 807.
[47] K. Momma, F. Izumi, VESTA 3 for three-dimensional visualization of crystal, volumetric and morphology data, J. Appl. Crystallogr. 44 (2011) 1272–1276.
[48] S. Mei, I. Knezevic, Thermal conductivity of ternary III-V semiconductor alloys: The role of mass difference and long-range order, J. Appl. Phys. 123 (2018) 125103.
[49] Springer Handbook of Condensed Matter and Materials Data. Eds. W. Martienssen and H. Warlimont. Springer Berlin Heidelberg New York 2005, p. 683.
[50] J.-Y. Zhang, X.-Y. Wang, L.Q. Min Xiao, X. Peng, Lattice contraction in free-standing CdSe nanocrystals, Appl. Phys. Lett. 81 (2002) 2076–2078.
[51] S. Nénon, https://github.com/sebnenon/VASP_tools.